Robotica (2023), **41**, pp. 277–291
doi:10.1017/S026357472200128X

CAMBRIDGE UNIVERSITY PRESS

RESEARCH ARTICLE

Clinically oriented ankle rehabilitation robot with a novel $\underline{R}-2\underline{U}PS/RR$ mechanism

Jianfeng Li[1], Yu Zhou[1], Mingjie Dong[1,*], Xi Rong[2] and Ran Jiao[1]

[1]Faculty of Materials and Manufacturing, Beijing University of Technology, Beijing, 100124, P.R. China and [2]the Affiliated Hospital of Qingdao University, Qingdao, 266000, P.R. China
*Corresponding author. E-mail: dongmj@bjut.edu.cn

Received: 5 April 2022; **Revised:** 19 July 2022; **Accepted:** 21 August 2022; **First published online:** 14 September 2022

Keywords: *R-2UPS/RR* , ankle rehabilitation robot, patient-passive exercise, trajectory tracking, patient-active exercise, spring model

Abstract

In order to make the designed ankle robotic system simpler, practical, and clinically oriented, we developed a novel $\underline{R}-2\underline{U}PS/RR$ ankle rehabilitation robot with a variety of training functions covering all the required ranges of motion of the ankle joint complex (AJC), where U, P, S, and R denote universal, prismatic, spherical, and revolute joints, respectively, and the underlined letter denotes the actuated joint. The robot was designed with three degrees of freedom (DOFs), with a series R mechanism and a $2\underline{U}PS/RR$ parallel mechanism. The main advantage is that the height of the robot is very low, which is convenient for clinical use by patients. At first, the mechanism design and inverse solution of positions were introduced in detail. Then, the patient-passive exercise based on the predefined trajectory tracking and patient-active exercise based on the spring model were developed to satisfy different rehabilitation stages. Finally, experiments with healthy subjects were conducted to verify the effectiveness of the developed patient-passive and patient-active exercises of the developed ankle rehabilitation robot, with results compared with the existing ankle robotic system showing good trajectory tracking performance and interactive performance.

1. Introduction

Robot-assisted rehabilitation has been a research hotspot in recent years, as the rehabilitation robot can replace the rehabilitation physician to carry on the long, repetitive, and intensive rehabilitation process [1]. For ankle rehabilitation, two types of robotic system have been developed the most, the wearable type and the platform type ankle devices, and research has shown that the wearable robots are more suitable for gait training while the platform type ankle devices are better suited for ankle exercises [2]. Therefore, many researchers have focused on platform type ankle devices. The most important point of designing a platform type ankle device is to be able to meet the ranges of motion (ROMs) of the ankle joint complex (AJC) in three degrees of freedom (DOFs); the ROM of the AJC in the directions of dorsiflexion/plantarflexion (DO/PL), inversion/eversion (IN/EV), and adduction/abduction (AD/AB) can be found in previous research [3].

There have been at least 16 platform type ankle devices no less than 2-DOFs that have been developed with different mechanism configurations and different actuator types [4–18]. In terms of DOFs of the mechanism, some of the platform type ankle devices have 3-DOFs to satisfy all the ROM of the AJC [3, 7, 12, 14, 15, 17–19], while some of them have only 2-DOFs to simplify the mechanism by eliminating the AD/AB motion [7, 9]. For the design of the platform type ankle devices, one important thing is to ensure that the rotation center of the robot coincides with that of the AJC which can avoid the secondary injury of the AJC to a certain extent [16, 20]; this also increases the size and complexity of the mechanism. Therefore, designing an ankle rehabilitation device with 3-DOFs and whereby the

mechanism's rotating center coincides with the AJC's rotating center, which also has a simple structure, enough workspace, ease of use, and small size, is a key problem in the mechanism design and optimization of ankle rehabilitation robot [1].

Rehabilitation training is different from the muscle strength training represented by isokinetic training [21]. Hence, for the ankle rehabilitation robot, one important thing is that the robot can drive the damaged AJC to perform high-precision passive rehabilitation training, performing a certain degree of rehabilitation training on the AJC's ROM and muscle strength [22]. From this point, the electrically driven ones have more advantages than pneumatic-driven ones, for the pneumatic muscle actuators (PMAs) can only pull and cannot push and the PMAs are highly nonlinear and require accurate modeling to be precisely controlled [23] although they have high power/volume ratios and intrinsic softness to enable joint compliance. At the same time, some general control strategies [24, 25] are proposed to increase the control accuracy or active adaptability of the parallel robot. The other important thing is to improve the enthusiasm of patients to participate in ankle rehabilitation training and ensure the safety of the rehabilitation training process. Therefore, many patient-active rehabilitation training methods have been developed based on impedance control or admittance control [20, 26–29], which have been verified to adaptively modify the predefined trajectory effectively based on real-time measurements of the human–robot interaction torque. Nevertheless, the computational complexity of the rehabilitation training methods based on impedance/admittance control is higher than those based on the first-order system, for they are both second-order system.

Therefore, we developed a clinically oriented ankle rehabilitation robot with a novel $\underline{R}-2\underline{U}PS/RR$ (R, U, P, S denote the revolute, universal, prismatic, and spherical joint, respectively, and the underlined letter denotes the actuated joint) mechanism, which is a series-parallel hybrid mechanism, and having a low height to be convenient for clinical use and can cover all the ROM of AJC, and its patient-active exercise is based on the first-order spring model to reduce computational complexity and improve real-time response of human–robot interaction.

The remainder of the paper is organized as follows. Section 2 describes the mechanism design and control of the $\underline{R}-2\underline{U}PS/RR$ ankle robotic system with its inverse solution of positions. The patient-passive exercise and patient-active exercise are presented in Section 3 and Section 4, respectively. Experiments and discussions of the developed patient-passive and patient-active exercises of the developed ankle rehabilitation robot are described in Section 5. Conclusions and future work are summarized in Section 6.

2. $\underline{R}$-2$\underline{U}PS/RR$ ankle robotic system

2.1. Mechanism design and control system

The mechanism design of the $\underline{R}-2\underline{U}PS/RR$ ankle rehabilitation robot (size: $546 \times 420 \times 376$ mm^3) is as in Fig. 1, which is a hybrid linkage mechanism composed of a rotating pair and a parallel mechanism in series. For the hybrid mechanism, the underlined letter denotes the actuated joint, and others denote passive joints. The mechanism consists of a series $\underline{R}$ mechanism and a $2\underline{U}PS/RR$ parallel mechanism, to ensure that the mechanism can meet the 3-DOFs of ankle rehabilitation training, namely DO/PL, IN/EV, and AD/AB, respectively. In addition, to ensure that patients of different sizes and different needs can be accommodated, we designed an angle adjusting mechanism to adjust the pitch angle of the mechanism.

As for the control system, two servo linear actuators (linear actuator PC25PA042B03-0150XF1, Thomson, USA, along with DC Servo motor SMH40-1030D8ENL-2, Kinavo, China) with rated power 100 W are employed as joints $\underline{P}_1$ and $\underline{P}_2$ to adjust the length of the kinematic chains with their stroke 150mm. An electric rotary table along with a DC Servo motor (SMH40-1030D10ENL-1, Kinavo, China) with rated power 100 W is used to drive the horizontal motion, which is a series R mechanism. The servo drives that we use for the three DC Servo motors are three DGFox DX060 drives (HDT, Italy), which have good interpolated position modes using the CANopen DS402 Protocol. A six-axis circular load cell (M3715C, SRI, China) is installed between the upper and lower parts of the moving

https://doi.org/10.1017/S026357472200128X Published online by Cambridge University Press

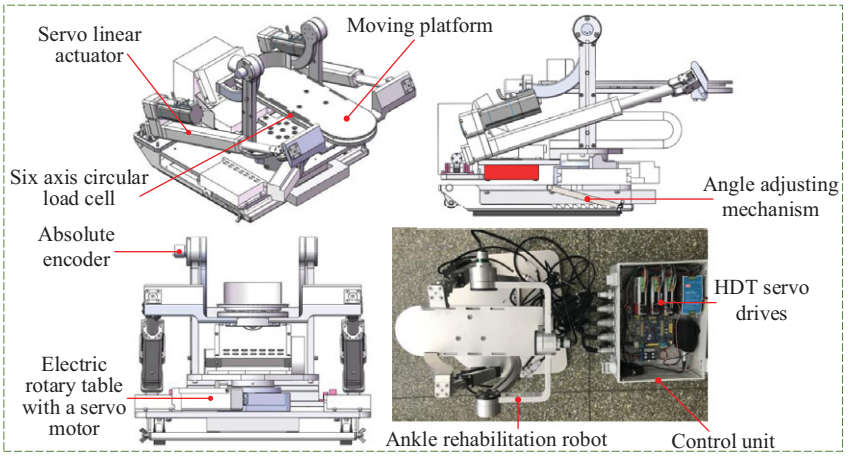

Figure 1. *Mechanism design of the* $\underline{R} - 2\underline{U}PS/RR$ *ankle robotic system.*

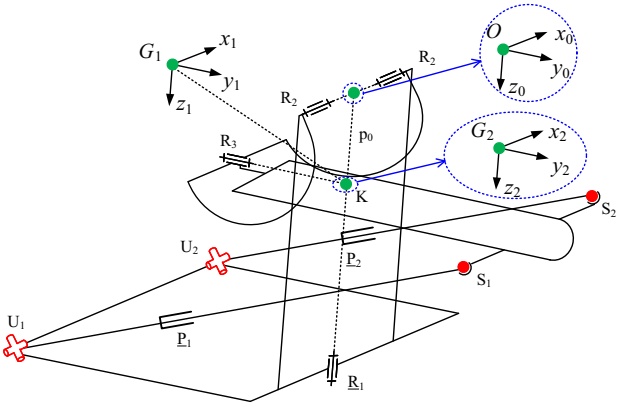

Figure 2. *Kinematic model and coordinate system of the mechanism. The blue dashed line box represents the reference directions of coordinates* $\{O\}$ *and* $\{G2\}$.

platform using a data acquisition card (M8128B1, SRI, China), while three absolute rotary encoders (P3022-V1-CW360, China) are employed to measure the rotation angle of each DOF and to detect the moving platform's trajectory in real time.

2.2. Inverse positions solution

The kinematic coordinate system of the $R - 2UPS/RR$ ankle rehabilitation robot is as in Fig. 2. The $2UPS/RR$ is a 2-DOF parallel mechanism, which can realize the rotating movement of the moving platform around the rotating pair R_2 and R_3 by connecting with the rotating pair R_1 in series. The rotating pair R_1 is fixed on the frame of the mechanism, which can realize the rotation movement of the entire $2UPS/RR$ parallel mechanism around the rotating pair R_1. Therefore, the mechanism has 3-DOFs and can achieve DO/PL, IN/EV, and AD/AB of the ankle joint.

The fixed coordinate system $\{O\}$ of the mechanism is established at the intersection of the rotation axes of the rotating pairs R_1 and R_2, and x_0 and z_0 coincide with the rotation axes of the rotating pairs R_2 and R_1, respectively; the direction of z_0 is downward along the axis of rotation, and the direction of y_0 is determined by the right-hand coordinate criterion.

https://doi.org/10.1017/S026357472200128X Published online by Cambridge University Press

In the initial position, let the intersection of the rotation axes of the rotation pairs R_1 and R_3 be the point K, and the distance from the point K to the origin O of the fixed coordinate system $\{O\}$ at this moment is p_0. The distance p_0 is the structure size of the organization and is a fixed value. However, the point K is no longer located at the intersection of the rotation axes of the rotation pairs R_1 and R_3 since the rotation axes of the rotation pairs R_1, R_2, and R_3 of the mechanism do not converge at one point when the movable platform of the mechanism performs DO/PL movement. When the moving platform of the mechanism performs DO/PL and IN/EV, the motion trajectory of point K is an arc with O as the origin in the y_0z_0 plane and p_0 as the radius.

The moving coordinate system $\{G_1\}$ is established at the point K, and the direction of z_1 is perpendicular to the moving platform downward. Initially, the directions of x_1, y_1, and z_1 coincide with the directions of x_0, y_0, and z_0, respectively. Here, we constrain the rotation of the moving coordinate system $\{G_1\}$ around the y_0 and z_0 axes of the fixed system $\{O\}$, so that it can only rotate around the x_0 axis of the fixed system $\{O\}$. The moving coordinate system $\{G_2\}$ is also established at point K, and y_2 coincides with the rotation axis of the rotating pair R_3. Initially, the directions of x_2, y_2, and z_2 are consistent with the directions of x_0, y_0, and z_0, respectively. Here, we constrain the rotation of the moving coordinate system $\{G_2\}$ around the x_1 and z_1 axes of the moving coordinate system $\{G_1\}$, so that it can only realize the rotation around the y_1 axis of the $\{G_1\}$.

The moving coordinate system $\{G_1\}$ and the moving coordinate system $\{G_2\}$ are both located on the moving platform, with their origins coinciding. At the initial position, the $\{G_1\}$ and $\{G_2\}$ are both consistent with the direction of the fixed coordinate system $\{O\}$.

Here, we define α as the rotation angle of the moving system $\{G_1\}$ around the x_0 axis of the fixed system $\{O\}$; define β as the rotation angle of the moving system $\{G_2\}$ around the y_1 axis of the moving system G1; and define γ as the rotation angle of the entire $2\underline{U}PS/RR$ parallel mechanism around the rotation pair R_1. Then, the rotation transformation matrix of the moving coordinate system $\{G_1\}$ relative to the fixed coordinate system $\{O\}$ can be expressed as in (1).

$$ {}^{O}_{G_1}R = R_{z_0}(0) \cdot R_{y_0}(0) \cdot R_{x_0}(\alpha) \tag{1} $$

The position vector of the moving coordinate system $\{G_1\}$ relative to the fixed coordinate system $\{O\}$ can be expressed as in (2).

$$ {}^{O}_{G_1}P = \begin{bmatrix} 0 & -p_0 \sin\alpha & p_0 \cos\alpha \end{bmatrix}^{\mathrm{T}} \tag{2} $$

The rotation transformation matrix of the moving coordinate system $\{G_2\}$ relative to the moving coordinate system $\{G_1\}$ can be expressed as in (3).

$$ {}^{G_1}_{G_2}R = R_{z_1}(0) \cdot R_{y_1}(\beta) \cdot R_{x_1}(0) \tag{3} $$

The position vector of the moving coordinate system $\{G_2\}$ relative to the moving coordinate system $\{G_1\}$ can be expressed as in (4).

$$ {}^{G_1}_{G_2}P = \begin{bmatrix} 0 & 0 & 0 \end{bmatrix}^{\mathrm{T}} \tag{4} $$

Then, the coordinate transformation matrix of the moving coordinate system $\{G_2\}$ relative to the fixed coordinate system $\{O\}$ is as in (5), where ${}^{O}_{G_2}R = {}^{O}_{G_1}R{}^{G_1}_{G_2}R$, and ${}^{O}_{G_2}P = {}^{O}_{G_1}P + {}^{G_1}_{G_2}P$.

$$ {}^{O}_{G_2}T = \begin{bmatrix} {}^{O}_{G_2}R & {}^{O}_{G_2}P \\ 0 & 1 \end{bmatrix} \tag{5} $$

For the reason that the S_1 and S_2 are the spherical joint centers on the moving platform, and U_1 and U_2 are the universal joint centers on the fixed base, then we can get the (6) based on the closed vector loop chain in Fig. 3.

$$ |l_i| = S_i - U_i \quad (i = 1, 2) \tag{6} $$

https://doi.org/10.1017/S026357472200128X Published online by Cambridge University Press

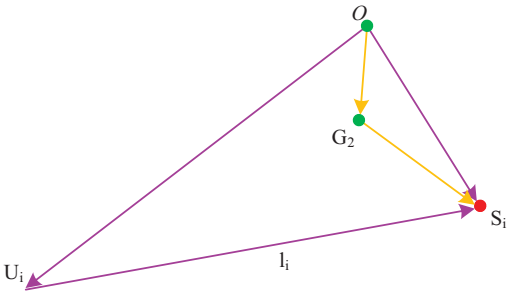

Figure 3. *The closed vector loop chain.*

where $S_i = {}^{O}_{G_2}RS_i' + {}^{O}_{G_2}P$, and S_i' is the position vector of the spherical joint center S_i in the moving coordinate system $\{G_2\}$. According to the designed mechanism, we can get (7).

$$\theta_1 = \gamma \tag{7}$$

By solving (6) and (7), the stroke of the two servo linear actuator l_1, l_2, and the rotation angle θ_1 of the electric rotary table can be obtained.

3. Patient-passive exercise based on trajectory tracking

At the early stage of ankle rehabilitation training in clinical practice, the patients must conduct patient-passive exercise to train their lost ROMs and regain some muscle strength. Therefore, the first step for ankle rehabilitation robot is to realize the patient-passive exercise, driving the disabled AJC to train along the predefined trajectories. For this $\underline{R} - 2\underline{U}PS/RR$ ankle rehabilitation robot consists of a series $\underline{R}$ mechanism and a $2\underline{U}PS/RR$ parallel mechanism, and its AD/AB movement is independent and decoupled from motion in the other two directions. Therefore, for this mechanism, the trajectory tracking control of passive rehabilitation training of the mechanism through the inverse solution of positions is relatively simple, and we have carried out single-axis patient-passive exercise and multi-axis linkage passive exercise, respectively.

3.1. Calculation optimization of inverse solution of positions

Traditional inverse solution of positions requires matrix operations, which can consume a large number of CPU. To reduce the computational complexity, we use the linear least squares method to fit the multidimensional data of the inverse solution result. As the rotation angle θ_1 of the electric rotary table is separate, we only need to fit the multidimensional data of the inverse solution of positions about the strokes of the two servo linear actuators l_1, l_2.

Define the general equation for the space curved surface as in (8). And, define the fitting equation as in (9).

$$l = a_{00} + a_{10}\theta_1 + a_{01}\theta_2 + a_{20}{\theta_1}^2 + a_{11}\theta_1\theta_2 + a_{02}{\theta_2}^2 \tag{8}$$

$$\begin{cases} f(\theta_1, \theta_2) = a_{00} + a_{10}\theta_1 + a_{01}\theta_2 + a_{20}{\theta_1}^2 + a_{11}\theta_1\theta_2 + a_{02}{\theta_2}^2 \\ f(\theta_1, \theta_2) = 0 \end{cases} \tag{9}$$

According to the definition of the least square method, the total fitting error V should be kept to a minimum.

$$\underset{\min}{V} = f(\theta_1, \theta_2) - l \tag{10}$$

https://doi.org/10.1017/S026357472200128X Published online by Cambridge University Press

Table I. *Parameter fitting value of the linear actuators.*

l_1	Parameter	a_{00}	a_{01}	a_{10}	a_{11}	a_{02}	a_{20}
	Fitting value	0.08857	2.663	−0.965	0.0337	−0.01464	0.008949
l_2	Parameter	a_{00}	a_{01}	a_{10}	a_{11}	a_{02}	a_{20}
	Fitting value	0.08857	2.663	0.965	−0.0337	−0.01464	0.008949

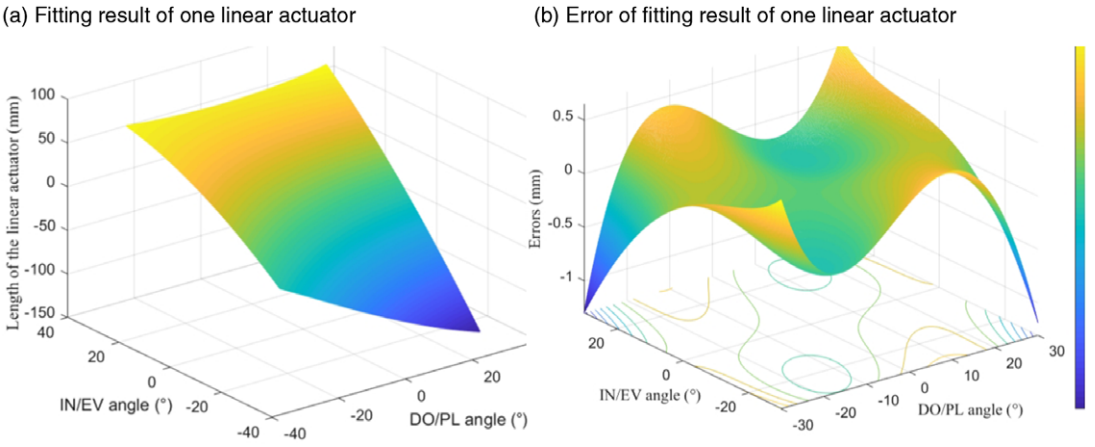

Figure 4. *Fitting results of the linear actuators' inverse solution of positions.*

(10) is a multi-component function, and the necessary condition for the existence of its minimum value is that its corresponding partial derivative is zero as in (11). The equation provides a unique solution. Thus, the fitting function is determined.

$$\frac{\partial V}{\partial a_{00}} = \frac{\partial V}{\partial a_{01}} = \frac{\partial V}{\partial a_{10}} = \frac{\partial V}{\partial a_{11}} = \frac{\partial V}{\partial a_{02}} = \frac{\partial V}{\partial a_{20}} = 0 \tag{11}$$

The surface fitting results of the two servo linear actuators based on their inverse solution of positions are as in Fig. 4, from which we can see that the result of the fitting is a saddle surface, which is smooth and the errors are within an acceptable range. The values of unknown parameters in the (9) are shown in Table I.

3.2. Single-axis and multi-axis passive exercise

In order to carry out patient-passive rehabilitation training for the AJC in an all-round way, we carried out single-axis passive rehabilitation training and multi-axis rehabilitation training based on the inverse solution of positions, respectively. The single-axis passive exercise is the reciprocating rehabilitation training in one of the DO/PL, IN/EV, or AD/AB directions. The AD/AB movement is driven by the electric rotary table, while the DO/PL and IN/EV are driven through the two servo linear actuators. The multi-axis rehabilitation training is to better train the flexibility and ROM of the AJC, and based on previous studies [20, 30, 31], spatial trajectories they proposed contain straight lines and arcs with different slopes, which can test the performance of the proposed robot and control algorithm. For this purpose, we developed six kinds of spatial trajectories, that is, circle, triangle, spatial straight line, semicircle, semicircle ring, and rectangle, which are all realized based on the inverse solution of positions. The passive exercise strategy in single-axis and multi-axis is as in Fig. 5.

The linear position interpolation of the single servo drives is shown in Fig 6. During the set time period ΔT, the driver follows point-to-point linear interpolation. Passive rehabilitation training is carried out by using the linear position interpolation mode of the DGFox DX060 servo drives, and the

https://doi.org/10.1017/S026357472200128X Published online by Cambridge University Press

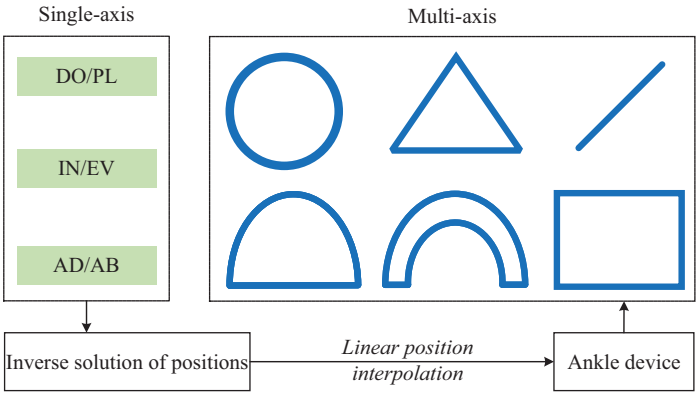

Figure 5. *Patient-passive strategy in single-axis and multi-axis.*

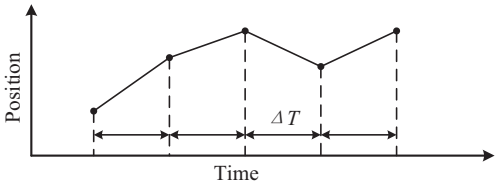

Figure 6. *Linear position interpolation.*

interpolation cycle is 8 ms. The upper computer sends control commands to the lower computer, which receives the control commands and controls the movement of the servo motors based on the CANopen DS402 protocol.

4. Patient-active exercise based on spring model

The patient-active exercise can stimulate the enthusiasm of patients to participate in ankle rehabilitation training, during which the AJC drives the robot to complete the corresponding tasks. The human–robot coupling system of the $\underline{R}-2\underline{U}PS/RR$ ankle rehabilitation robot is equivalent to a mass-spring-damp system as in (12), where T is the human–robot interaction torque, M is the mass, K is the stiffness coefficient, B represents the damping coefficient, and θ is the rotating angle.

$$T(t)-K\theta(t)-B\frac{d\theta(t)}{dt}=M\frac{d\theta^2(t)}{dt^2} \tag{12}$$

For the reason that the running speed of the $\underline{R}-2\underline{U}PS/RR$ ankle rehabilitation robot is slow and almost uniform during the rehabilitation process, its angular acceleration can be approximately zero, that is, $\frac{d\theta^2(t)}{dt^2}=0$. In addition, the response speed of the underdamped second-order system is a little slow with high computational complexity, especially using the proportional and time-shifting methods [20]. Therefore, we simplified the human–robot coupling system model into a first-order spring model [32, 33], as in (13), which can reduce computational complexity and increase the real-time performance.

$$T(t)=K\theta(t) \tag{13}$$

In the patient-active exercise mode, the $\underline{R}-2\underline{U}PS/RR$ ankle rehabilitation robot uses only three torques, T_x, T_y, and T_z, which are measured from the six-axis circular load cell M3715C. To make the obtained interaction torque smooth, stable, and accurate, we adopt the sorting average filtering method, during which every ten numbers are taken and sorted by using bubble sort, and the average of the five

https://doi.org/10.1017/S026357472200128X Published online by Cambridge University Press

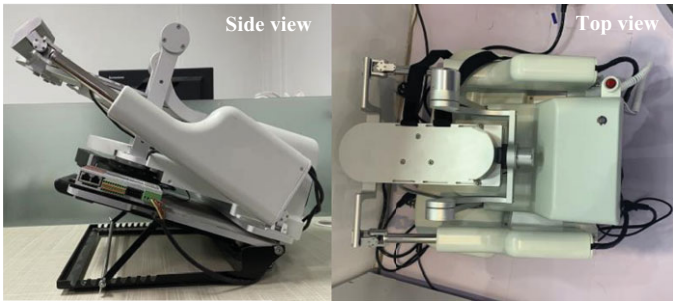

Figure 7. *Prototype of the developed $\underline{R}-2\underline{U}PS/RR$ ankle robotic system.*

numbers in the middle is taken as the current measured interaction torque. The coefficient K is adapted according to experiments and physicians' experience, then the deduced deviations in angles θ (t) can be obtained according to (13), and mapped into the joint space based on the inverse solution of positions and realized by using the linear position interpolation of the servo drives.

5. Experiments and discussions

To evaluate the effectiveness of the developed $\underline{R}-2\underline{U}PS/RR$ ankle rehabilitation robot, we conducted experiments with five healthy subjects. The subjects signed informed consent before the experiments. All experiments were approved by the Ethical Committee of Beijing University of Technology and conformed to the Declaration of Helsinki. The prototype of the developed $\underline{R}-2\underline{U}PS/RR$ ankle robotic system is as in Fig. 7; the left one is the side view without the shell while the right one is the top view with shell. The developed patient-passive exercise and the patient-active exercise were tested.

5.1. Experiments of the patient-passive exercise

For the reason that the AD/AB movement is independent and decoupled from motion in the other two directions, driven by the electric rotary table, and also the patient-passive exercises in DO/PL and IN/EV are just realized through different combination drive forms of the two servo linear actuators, we only tested the single-axis patient-passive exercise in DO/PL direction, while for the multi-axis patient-passive exercise, the trajectories of circle, triangle, spatial straight line, semicircle, semicircle ring, and rectangle were all tested with healthy subjects. It should be noted that in order to facilitate the drawing of the spatial curve, we only generate the predetermined trajectories through the combined motion around the $x-axis$ and the $z-axis$. And it is important to note that, for the toe of the AJC, the trajectory of the movement around the $x-axis$ and the movement around the $z-axis$ in space is on a spherical surface, for the reason that the $x-axis$ and the $z-axis$ intersect at one point.

5.1.1. Passive exercise in DO/PL direction

The trajectories of the rehabilitation training are predefined, and reciprocating movement is performed within the AJC's ROM. Experimental result of patient-passive exercise in DO/PL from one subject is as in Fig. 8, where the sampling frequency is 10 Hz, the desired value is the predefined trajectory while the actual value is the actual trajectory. It should be noted that, unlike most passive rehabilitation training that uses sine or cosine functions as the predefined trajectories, we use a passive training trajectory with constant velocity characteristics to improve the effectiveness of rehabilitation training; the speed remains constant in most of the time, while the speed becomes 10% of the original value when there is 2° left before the movement reaches the threshold.

From the results we can see that the actual trajectories of the patient-passive exercise in DO/PL direction are almost identical to the predefined trajectories, showing good trajectory tracking performance.

https://doi.org/10.1017/S026357472200128X Published online by Cambridge University Press

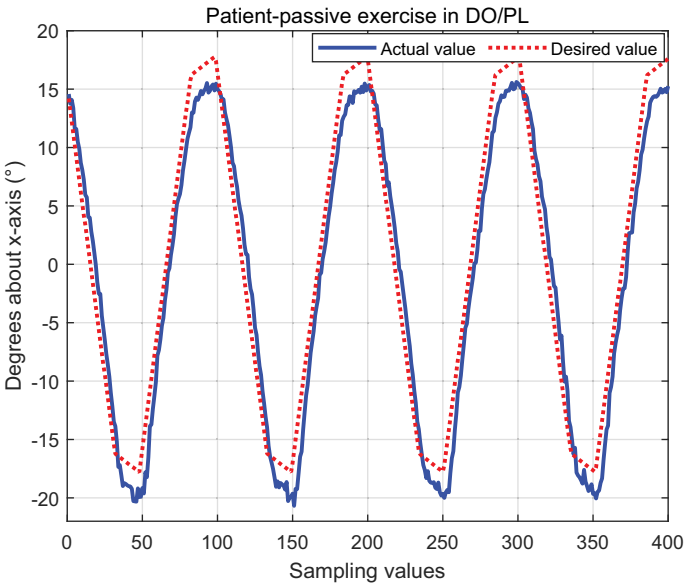

Figure 8. *Patient-passive exercise in DO/PL direction.*

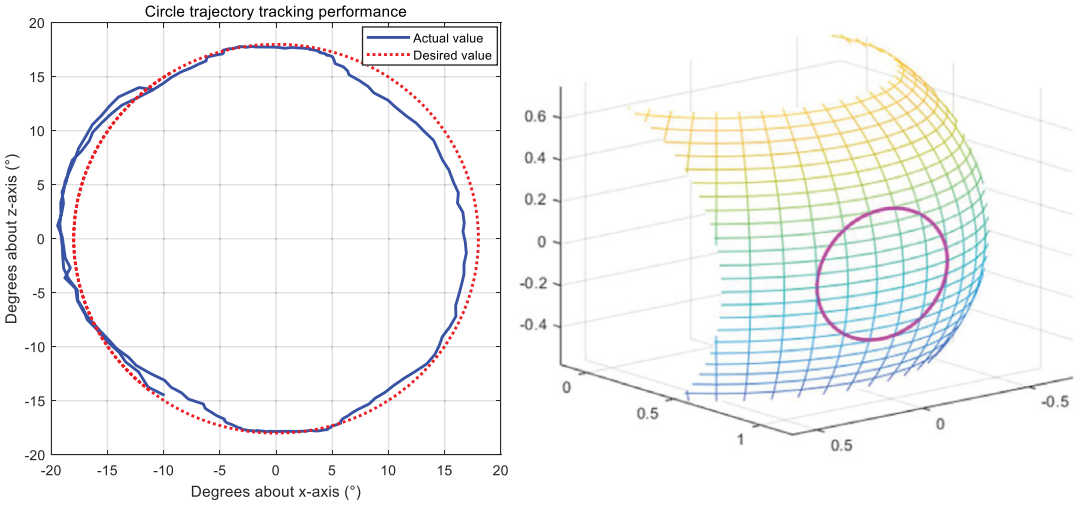

Figure 9. *Circle trajectory tracking performance.*

5.1.2. Circle trajectory

The circle trajectory is through the combined motion around the $x-axis$ and the $z-axis$, with the DO/PL and AD/AB all range from $-18^\circ \sim 18^\circ$. The result of one subject is as in Fig. 9, where the left figure is the plane representation of the experimental result while the right one is its spatial representation on the spherical surface with the unit of the coordinate system radian. The desired value is the predefined trajectory while the actual value is the actual trajectory.

From Fig. 9 we can see that the robot can drive the AJC along with the predefined trajectory with very high precision, showing very good trajectory tracking performance.

5.1.3. Triangle trajectory

The triangle trajectory is also through the combined motion around the $x-axis$ and the $z-axis$, with the DO/PL ranges from $-18^\circ \sim 18^\circ$ while the AD/AB ranges from $-20^\circ \sim 20^\circ$. Result of one subject

https://doi.org/10.1017/S026357472200128X Published online by Cambridge University Press

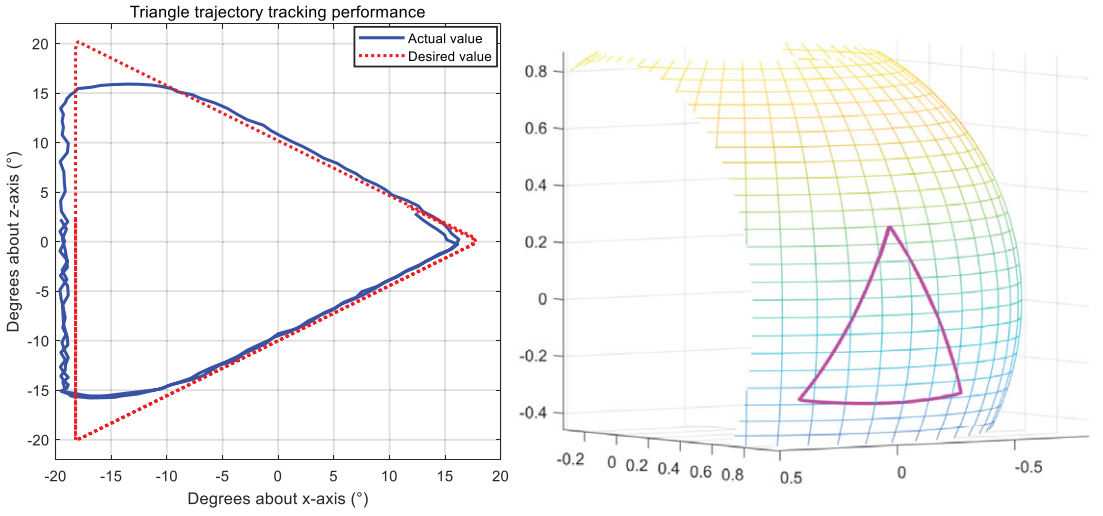

Figure 10. *Triangle trajectory tracking performance.*

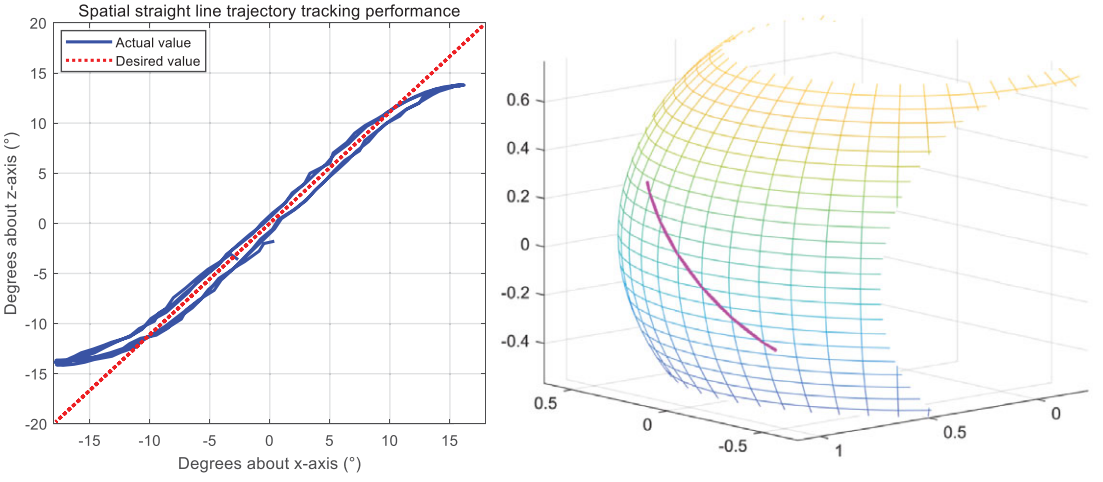

Figure 11. *Spatial straight line trajectory tracking performance.*

including both the plane representation and spatial representation on the spherical surface is shown as in Fig. 10.

5.1.4. Spatial straight line trajectory

The spatial straight line trajectory is also through the combined motion around the $x-axis$ and the $z-axis$, with the DO/PL ranges from $-18^\circ \sim 18^\circ$ while the AD/AB ranges from $-20^\circ \sim 20^\circ$. Result of one subject including both the plane representation and spatial representation on the spherical surface is shown as in Fig. 11.

5.1.5. Semicircle trajectory

The semicircle trajectory is also through the combined motion around the $x-axis$ and the $z-axis$, with the DO/PL ranges from $0^\circ \sim 18^\circ$ while the AD/AB ranges from $-18^\circ \sim 18^\circ$. The radius of the semicircle is 18°. Result of one subject including both the plane and spatial representation is shown as in Fig. 12.

https://doi.org/10.1017/S026357472200128X Published online by Cambridge University Press

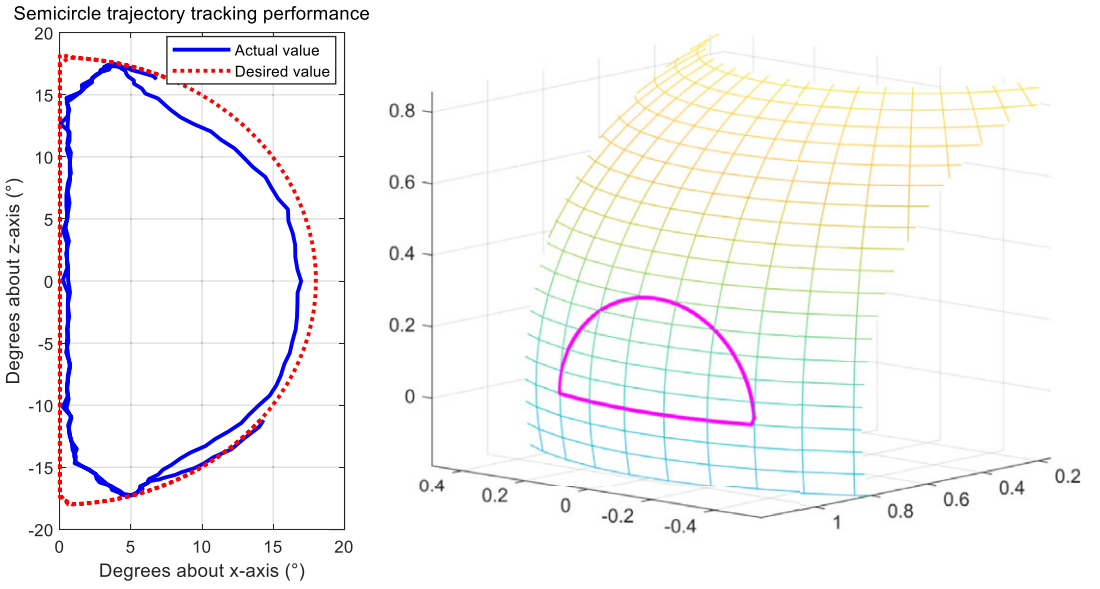

Figure 12. *Semicircle trajectory tracking performance.*

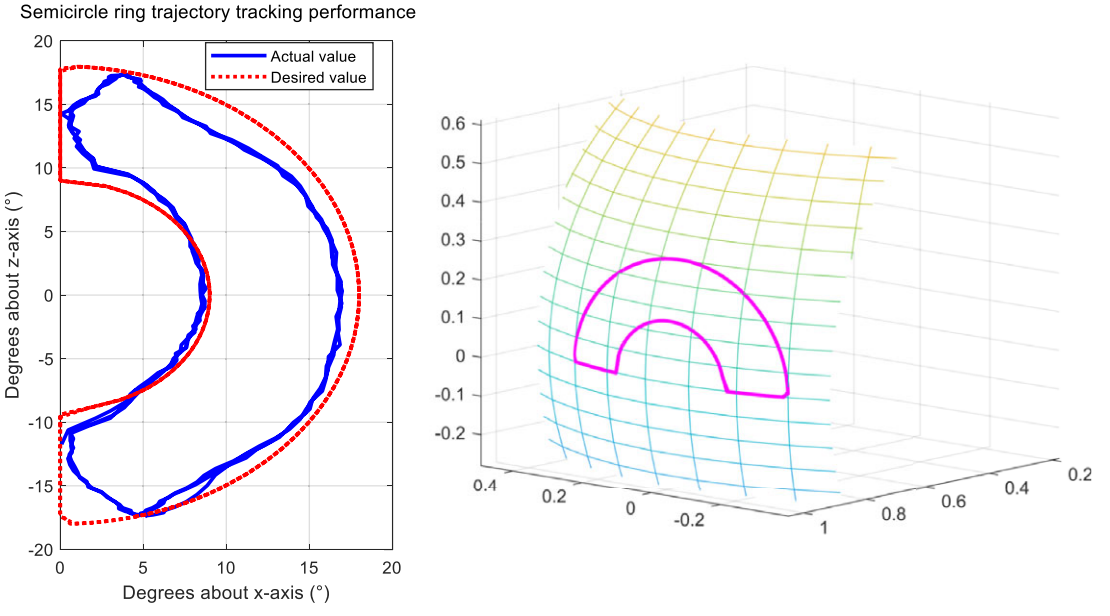

Figure 13. *Semicircle ring trajectory tracking performance.*

5.1.6. Semicircle ring trajectory

The semicircle ring trajectory is also through the combined motion around the $x-axis$ and the $z-axis$, with the DO/PL ranges from $0^\circ \sim 18^\circ$ while the AD/AB ranges from $-18^\circ \sim 18^\circ$. The radius of the inner ring and the outer ring is 9° and 18°, respectively. Result of one subject including both the plane representation and spatial representation on the spherical surface is shown as in Fig. 13.

5.1.7. Rectangle trajectory

The rectangle trajectory is also through the combined motion around the $x-axis$ and the $z-axis$, with the DO/PL ranges from $-18^\circ \sim 18^\circ$ while the AD/AB ranges from $-20^\circ \sim 20^\circ$. Result of one subject

https://doi.org/10.1017/S026357472200128X Published online by Cambridge University Press

Table II. *Evaluation of results in patient-passive exercise experiments.*

	Metrics	**MD (°)**	**RMSD (°)**
Patient-passive exercise	DO/PL	2.6070	2.7693
	Circle	1.0768	1.2583
	Triangle	1.4701	1.9039
	Spatial straight line	1.8853	2.5170
	Semicircle	1.1767	1.4632
	Semicircle ring	1.1607	1.4467
	Rectangle	1.5310	1.7915

MD, mean deviation; RMSD, root mean square deviation.

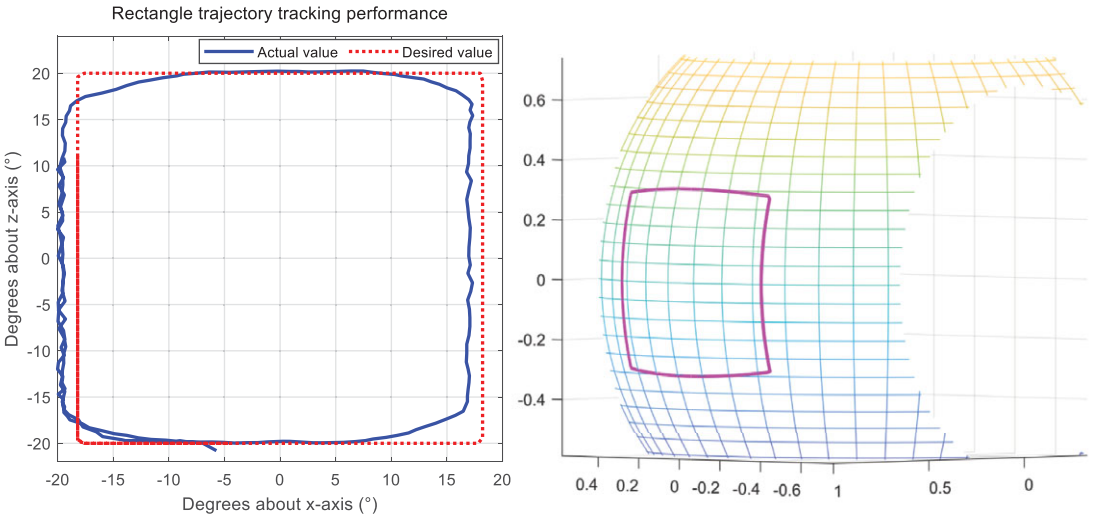

Figure 14. *Rectangle trajectory tracking performance.*

including both the plane representation and spatial representation on the spherical surface is shown as in Fig. 14.

5.1.8. Results of the patient-passive exercise experiments

From Figs. 8, 9, 10, 11, 12, 13, and 14 we can see that the ankle rehabilitation robot basically moves according to the predetermined trajectories in space on a spherical surface. To further quantitatively evaluate the performance of the developed patient-passive exercise, we calculated the mean deviation (MD) and root-mean-square deviation (RMSD) of the trajectory tracking results between the predicted trajectory and the actual trajectory in all the experiments, where $MD = \frac{\sum_{i=1}^{n} |\theta_p - \theta_a|}{n}$, $RMSD = \sqrt{\frac{\sum_{i=1}^{n} (\theta_p - \theta_a)^2}{n}}$, θ_a and θ_p represent the actual and desired trajectories, respectively. The results is as in Table II, from which we can see that although the errors in the separate $x-axis$ and $z-axis$ directions are visually large, the error after space vector synthesis is not large compared with our previous work [22], reflecting better trajectory tracking performance.

5.2. Experiments of the patient-active exercise

For the reason that the amount of IN/EV movement is very small, and it is rarely used in normal times and can basically be ignored, during the patient-active exercise, we also try to use only the combined motion around the $x-axis$ and the $z-axis$, to give a better display on a spherical surface. During the

https://doi.org/10.1017/S026357472200128X Published online by Cambridge University Press

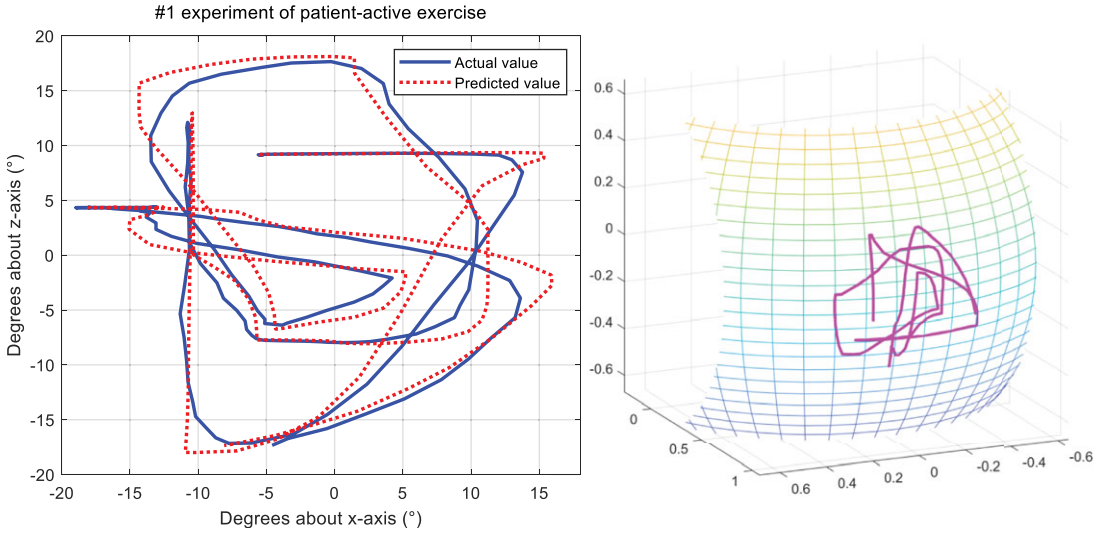

Figure 15. *#1 experiment of patient-active exercise.*

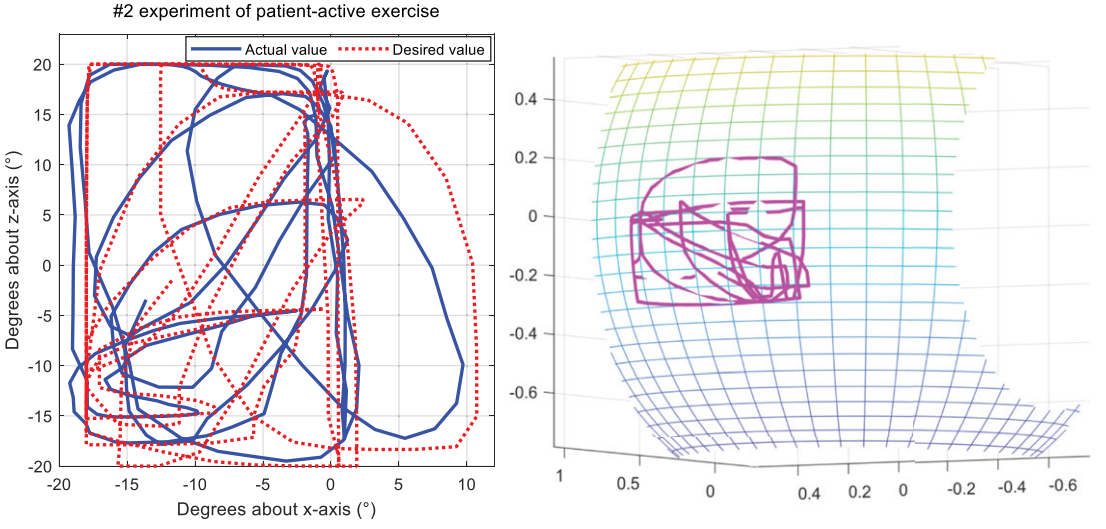

Figure 16. *#2 experiment of patient-active exercise.*

experiments, we constrained the movement in the direction of IN/EV, with the experimental results of two patient-active exercises are as in Figs. 15 and 16, respectively, where the predicted value is deduced based on the patient-active exercise strategy in (13) while the actual value is the actual trajectory of the robot.

From Fig. 15 and 16, we can see that the actual trajectories can basically move according to the deduced trajectories obtained from (13) in space on a spherical surface. To quantitatively evaluate the performance of the developed patient-active exercise, we also calculated the mean deviation (MD) and root-mean-square deviation (RMSD) of the trajectory tracking results between the predicted trajectory and the actual trajectory in all the experiments, with the results shown in Table III.

From Table III, we can see that the error after space vector synthesis is also very small. What needs special explanation is that the position reaching the limit $\pm 20^{\circ}$ shown in Fig. 16 is the effect of the software limit we set, which is to protect the AJC's safety during rehabilitation training.

https://doi.org/10.1017/S026357472200128X Published online by Cambridge University Press

Table III. *Evaluation of results in patient-active exercise experiments.*

	Metrics	**MD (°)**	**RMSD (°)**
Patient-active exercise	#1 experiment	1.5381	2.0162
	#2 experiment	2.7962	3.8054

6. Conclusions and future work

In this paper, we developed a novel 3-DOF $\underline{R} - 2\underline{U}PS/RR$ ankle rehabilitation robot, which was designed with a series $\underline{R}$ mechanism and a $2\underline{U}PS/RR$ parallel mechanism. The main contributions of the work include: 1) the height of the robot is very low, which is convenient for clinical application; 2) the calculation of inverse solution of position is optimized to reduce the computational complexity by using linear least squares method; and 3) the human–robot coupling system model is simplified into a first-order spring model to further reduce computational complexity and increase the real-time performance. Also, the patient-passive exercise and patient-active exercise were developed with healthy subjects involved to verify their effectiveness, showing both good trajectory tracking performance.

Future research will focus on the development of more rehabilitation training methods, such as isokinetic training and proprioceptive training, as well as quantitative evaluation of ankle rehabilitation and intelligent training prescription. In addition, a large number of tests with healthy subjects will be conducted to verify the safety, stability, and effectiveness of the entire system, to ensure that its performance and stability are good enough for ankle disabled patients, so as to conduct clinical trials as soon as possible.

Authors' contributions. Jianfeng Li and Mingjie Dong conceived and designed this study. Yu Zhou and Ran Jiao performed the mechanical design of the mechanism and completed the control system. Jianfeng Li and Yu Zhou conducted the kinematic analysis. Yu Zhou and Xi Rong wrote the paper. Jianfeng Li, Mingjie Dong, and Xi Rong reviewed and edited the manuscript. All authors had read and approved the manuscript.

Financial support. This work was supported in part by the National Natural Science Foundation of China under Grants No. 61903011 and No. 52175001, and in part by the General Program of Science and Technology Development Project of Beijing Municipal Education Commission under Grant No. KM202010005021.

Conflicts of interest. The authors declare that the research was conducted in the absence of any commercial or financial relationships that could be construed as a potential conflict of interest.

Ethical considerations. No ethical issue with this paper.

References

[1] M. Dong, Y. Zhou, J. Li, X. Rong, W. Fan, X. Zhou and Y. Kong, "State of the art in parallel ankle rehabilitation robot: A systematic review," *J. NeuroEng. Rehabil.* **18**(1), 1–15 (2021).

[2] M. Zhang, T. C. Davies and S. Xie, "Effectiveness of robot-assisted therapy on ankle rehabilitation A systematic review," *J. NeuroEng. Rehabil.* **10**(1), 1–16 (2013).

[3] C. Wang, Y. Fang, S. Guo and C. Zhou, "Design and kinematic analysis of redundantly actuated parallel mechanisms for ankle rehabilitation," *Robotica* **33**(2), 366–384 (2015).

[4] M. Girone, G. Burdea, M. Bouzit, V. Popescu and J. E. Deutsch, "Orthopedic rehabilitation using the "Rutgers ankle" interface," *Med. Meets Virt. Reality* **89**, 2000–2095 (2000).

[5] J. Yoon and J. Ryu, "A New Family of 4-DOF Parallel Mechanisms (1T-3R and 2T-2R) with Two Platforms and Its Application to A Footpad Device," **In:** *International Design Engineering Technical Conferences and Computers and Information in Engineering Conference*, Salt Lake City, Utah (2004) pp. 257–265.

[6] J. Yoon and J. Ryu, "A Novel Reconfigurable Ankle/foot Rehabilitation Robot," **In:** *Proceedings of the IEEE International Conference on Robotics and Automation*, Barcelona, Spain (2005), pp. 2290–2295.

[7] G. Liu, J. Gao, H. Yue, X. Zhang and G. Lu, "Design and Kinematics Analysis of Parallel Robots for Ankle Rehabilitation," **In:** *IEEE/RSJ International Conference on Intelligent Robots and Systems*, Beijing, China (2006), pp. 253–258.

https://doi.org/10.1017/S026357472200128X Published online by Cambridge University Press

[8] M. Malosio, S. P. Negri, N. Pedrocchi, F. Vicentini, M. Caimmi and L. M. Tosatti, "A Spherical Parallel Three Degrees-of-freedom Robot for Ankle-Foot Neuro-Rehabilitation," **In:** *Annual International Conference of the IEEE Engineering in Medicine and Biology Society*, San Diego, CA (2012) pp. 3356–3359.
[9] M. S. Ayas, I. H. Altas and E. Sahin, "Fractional order based trajectory tracking control of an ankle rehabilitation robot," *Trans. Inst. Meas. Control* **40**(2), 550–564 (2018).
[10] H. Rakhodaei, M. Saadat, A. Rastegarpanah and C. Z. Abdullah, "Path planning of the hybrid parallel robot for ankle rehabilitation," *Robotica* **34**(1), 173–184 (2016).
[11] Q. Ai, C. Zhu, J. Zuo, W. Meng, Q. Liu, S. Q. Xie and M. Yang, "Disturbance-estimated adaptive backstepping sliding mode control of a pneumatic muscles-driven ankle rehabilitation robot," *Sensors* **18**(1), 66 (2017).
[12] P. K. Jamwal, S. Xie and K. C. Aw, "Kinematic design optimization of a parallel ankle rehabilitation robot using modified genetic algorithm," *Robot. Auton. Syst.* **57**(10), 1018–1027 (2009).
[13] P. K. Jamwal and S. Hussain, "Multicriteria design optimization of a parallel ankle rehabilitation robot: fuzzy dominated sorting evolutionary algorithm approach," *IEEE Trans. Syst. Man Cybern. -Syst.* **46**(5), 589–597 (2015).
[14] M. Zhang, J. Cao, G. Zhu, Q. Miao, X. Zeng and S. Q. Xie, "Reconfigurable workspace and torque capacity of a compliant ankle rehabilitation robot (CARR)," *Robot. Auton. Syst.* **98**(4), 213–221 (2017).
[15] P. K. Jamwal, S. Q. Xie, Y. H. Tsoi and K. C. Aw, "Forward kinematics modelling of a parallel ankle rehabilitation robot using modified fuzzy inference," *Mech. Mach. Theory* **45**(11), 1537–1554 (2010).
[16] C. Wang, Y. Fang, S. Guo and Y. Chen, "Design and kinematical performance analysis of a 3-RUS/RRR redundantly actuated parallel mechanism for ankle rehabilitation," *J. Mech. Robot.* **5**(4), 041003 (2013).
[17] M. Vallés, J. Cazalilla, Á. Valera, V. Mata, Á. Page and M. Díaz-Rodríguez, "A 3-PRS parallel manipulator for ankle rehabilitation: towards a low-cost robotic rehabilitation," *Robotica* **35**(10), 1939–1957 (2017).
[18] J. Li, S. Zuo, L. Zhang, M. Dong, Z. Zhang, C. Tao and R. Ji, "Mechanical design and performance analysis of a novel parallel robot for ankle rehabilitation," *J. Mech. Robot.* **12**(5), 051007 (2020).
[19] S. Zuo, J. Li, M. Dong, X. Zhou, W. Fan and Y. Kong, "Design and performance evaluation of a novel wearable parallel mechanism for ankle rehabilitation,"," *Front. Neurorobotics* **14**, 9 (2020).
[20] M. Dong, W. Fan, J. Li, X. Zhou, X. Rong, Y. Kong and Y. Zhou, "A new ankle robotic system enabling whole-stage compliance rehabilitation training," *IEEE-ASME Trans. Mechatron.* **26**(3), 1490–1500 (2021).
[21] J. Li, Y. Zhou, M. Dong and X. Rong, "Isokinetic muscle strength training strategy of an ankle rehabilitation robot based on adaptive gain and cascade PID control," *IEEE Trans. Cogn. Dev. Syst.*, 1–1 (2022). doi: 10.1109/TCDS.2022.3145998.
[22] J. Li, W. Fan, M. Dong and X. Rong, "Implementation of passive compliance training on a parallel ankle rehabilitation robot to enhance safety," *Ind. Robot.* **47**(5), 747–755 (2020).
[23] M. Zhang, A. McDaid, A. J. Veale, Y. Peng and S. Q. Xie, "Adaptive trajectory tracking control of a parallel ankle rehabilitation robot with joint-space force distribution," *IEEE Access* **7**, 85812–85820 (2019).
[24] N. Ma, X. Dong and D. Axinte, "Modeling and experimental validation of a compliant underactuated parallel kinematic manipulator," *IEEE-ASME Trans. Mechatron.* **25**(3), 1409–1421 (2020).
[25] B. Zhong, K. Guo, H. Yu and M. Zhang, "Toward gait symmetry enhancement via a Cable-Driven exoskeleton powered by series elastic actuators," *IEEE Robot. Autom. Lett.* **7**(2), 786–793 (2022).
[26] J. A. Saglia, N. G. Tsagarakis, J. S. Dai and D. G. Caldwell, "Control strategies for patient-assisted training using the ankle rehabilitation robot (ARBOT)," *IEEE-ASME Trans. Mechatron.* **18**(6), 1799–1808 (2012).
[27] P. K. Jamwal, S. Hussain, M. H. Ghayesh and S. V. Rogozina, "Impedance control of an intrinsically compliant parallel ankle rehabilitation robot," *IEEE Trans. Ind. Electron.* **63**(6), 3638–3647 (2016).
[28] M. Dong, J. Li, X. Rong, W. Fan, Y. Kong and Y. Zhou, "Compliant Physical Interaction to Enhance Rehabilitation Training of A Parallel Ankle Robotic System," **In:** *Chinese Automation Congress (CAC)*, Shanghai, China (2020) pp. 2191–2196.
[29] M. Zhang, S. Q. Xie, X. Li, G. Zhu, W. Meng, X. Huang and A. J. Veale, "Adaptive patient-cooperative control of a compliant ankle rehabilitation robot (CARR) with enhanced training safety," *IEEE Trans. Ind. Electron.* **65**(2), 1398–1407 (2017).
[30] E. P. Washabaugh, J. GuoK. C., Chang, C. D. Remy and C. Krishnan, "A portable passive rehabilitation robot for upper-Extremity functional resistance training," *IEEE Trans. Biomed. Eng.* **66**(2), 496–508 (2019).
[31] Y. RenY. N. WuC. Y. Yang, T. XuR. L. Harvey and L. Q. Zhang, "Developing a wearable ankle rehabilitation robotic device for in-Bed acute stroke rehabilitation," *IEEE Trans. Neural Syst. Rehabil. Eng.* **25**(6), 589–596 (2017).
[32] Q. Wu, X. Wang, B. Chen and H. Wu, "Development of a Minimal-Intervention-Based admittance control strategy for upper extremity rehabilitation exoskeleton," *IEEE Trans. Syst. Man Cybern. Syst.* **48**(6), 1005–1016 (2018).
[33] C. Xie, Q. Yang, Y. Huang, S. W. Su, T. Xu and R. Song, "A hybrid Arm-Hand rehabilitation robot with EMG-Based admittance controller," *IEEE Trans. Biomed. Circuits Syst.* **15**(6), 1332–1342 (2021).

Cite this article: J. Li, Y. Zhou, M. Dong, X. Rong, R. Jiao (2023). "Clinically oriented ankle rehabilitation robot with a novel $\underline{R}-2\underline{U}PS/RR$ mechanism", Robotica **41**, 277–291. https://doi.org/10.1017/S026357472200128X